

Sampling functions for multimode homodyne tomography with a single local oscillator

Jaromír Fiurášek

*Department of Chemical Physics, The Weizmann Institute of Science, Rehovot 76100, Israel
and Department of Optics, Palacký University, 17. listopadu 50, 772 07 Olomouc, Czech Republic
(November 21, 2018)*

We derive various sampling functions for multimode homodyne tomography with a single local oscillator. These functions allow us to sample multimode s -parametrized quasidistributions, density matrix elements in Fock basis, and s -ordered moments of arbitrary order directly from the measured quadrature statistics. The inevitable experimental losses can be compensated by proper modification of the sampling functions. Results of Monte Carlo simulations for squeezed three-mode state are reported and the feasibility of reconstruction of the three-mode Q -function and s -ordered moments from 10^7 sampled data is demonstrated.

PACS number(s): 42.50.Dv, 03.65.-w

I. INTRODUCTION

Recent development of quantum-state reconstruction methods has made it possible to completely reconstruct an unknown state of a quantum mechanical system provided that many identical copies of the state are available. The method was pioneered in quantum optics, where an optical homodyne tomography was devised to reconstruct a quantum state of traveling electromagnetic field [1–4]. Other proposed techniques involved unbalanced homodyning [5] and cavity-field measurements by atomic probes [6]. Quantum-state reconstruction procedures were also successfully applied to molecular vibrational state [7] and motional quantum state of trapped ion [8].

Single-mode optical homodyne tomography is now a well-established technique. Based on balanced homodyne detection, the method seeks to reconstruct the quantum state from the statistics of the quadrature components of the signal mode. The standard experimental setup involves balanced lossless beam splitter, where the signal is mixed with a strong coherent local oscillator (LO). Two photodetectors are placed at the beam splitter outputs and the two photocurrents are subtracted, thereby removing LO fluctuations from the resulting signal.

Wigner function can be obtained from the measured quadrature statistics by means of inverse Radon transform [9,1]. Once the Wigner function is known, expectation value of any operator can be evaluated by averaging corresponding phase-space function over the Wigner quasidistribution. This strategy, however, is not optimal, because the experimental errors are amplified during numerical data processing and the final error can be very large. Fortunately, the detour via Wigner function can be avoided and density matrix elements in Fock basis can be directly reconstructed by averaging appropriate sampling functions over the measured quadrature statistics [10–15]. The functions for sampling s -ordered moments were found in [16–18], and those allowing direct reconstruction of the exponential moments of quantum phase

distributions were obtained in [19,20] (for a review, see [21,22]). The problems with inverse Radon transform can be avoided by reconstructing smoothed Wigner functions [23]. The sampling is a simple and straightforward linear operation which can be in principle performed in real time during experiment. We note that, besides linear sampling procedures, reconstruction strategies based on maximum likelihood estimation [24] and maximum entropy principle [25] have been proposed.

Recently, increasing attention has been devoted to multimode homodyne tomography [26–32], because some of the most interesting quantum mechanical phenomena stem from correlations between several degrees of freedom. Let us mention just the EPR paradox and violation of Bell’s inequalities [33]. Quantized electromagnetic field is one of the most suitable systems for thorough investigation and exploitation of these phenomena. For example, entangled signal and idler photons can be routinely prepared by means of spontaneous parametric down-conversion [34]. The entangled photon pairs play crucial role in certain quantum state teleportation schemes [35] and quantum cryptography setups [36].

Multimode extension of optical homodyne tomography is straightforward. One can introduce a separate LO and homodyne detector for each mode of interest and measure joint multimode quadrature distribution. In this case the sampling functions developed for single-mode tomography can be immediately employed. Very recently, this approach has been used to measure the joint photon number statistics of two-mode squeezed state prepared in a nondegenerate optical parametric amplifier [4].

However, the requirement of specific homodyne detector for each mode complicates the experiment. It would often be much more feasible to use only one homodyne detector and one LO. In such experiment, a distribution of one quadrature X , which is a linear superposition of N single-mode quadratures, is measured. The knowledge of the probability distribution of all distinct quadratures X provides a complete information on the multimode quantum state. In particular, two-mode tomography

arXiv:quant-ph/0006023v1 5 Jun 2000

with single homodyne detector was discussed extensively. The functions for sampling density matrix elements in Fock basis were found in [27,28,31], and those allowing direct reconstruction of two-mode correlation functions were obtained in [29–31]. Recently, a general multimode homodyne tomography with a single LO was considered and the sampling functions for density matrix elements were expressed in terms of integrals [32]. In this paper we shall derive various important sampling functions for multimode homodyne tomography with a single LO. All functions are expressed in analytical form. Imperfect detection is considered and it is shown that the losses can be compensated by proper modification (rescaling) of the sampling functions.

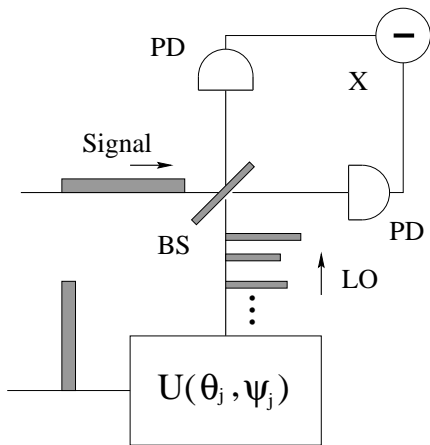


FIG. 1. Measurement of internal quantum correlations of optical pulses [29]. The signal pulse and a train of strong local-oscillator (LO) pulses that are short compared to the signal pulse are mixed at a 50%:50% beam splitter (BS) and the two photocurrents measured by photodetectors (PD) are subtracted. The train of LO pulses is prepared interferometrically, thereby allowing one to control the pulse distances, relative phases and intensities, as symbolically denoted by $U(\theta_j, \psi_j)$.

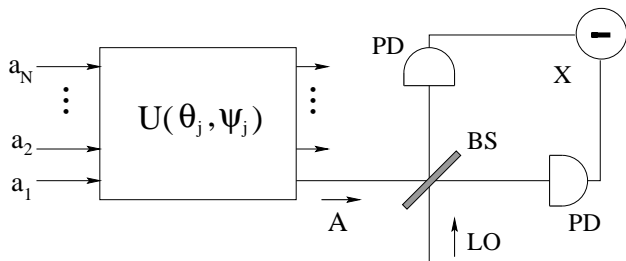


FIG. 2. Optical homodyne tomography of single-frequency multimode optical field. The signal modes a_1, \dots, a_N feed the input of N -port interferometer which prepares the mode A at one of its outputs. Subsequently, the distribution of quadrature X is measured by means of standard single-mode homodyne detection.

The paper is organized as follows. In Sec. II we address the reconstruction of multimode smoothed Wigner functions. The results are then applied in Sec. III to find the sampling functions for density matrix elements in Fock basis. The reconstruction of s -ordered moments of the field operators is discussed in Sec. IV. The results of Monte Carlo simulations of multimode homodyne tomography are reported in Sec. V. Finally, Section VI contains conclusions.

II. SAMPLING FUNCTIONS FOR S -PARAMETRIZED QUASIDISTRIBUTIONS

In multimode homodyne tomography with a single local oscillator one measures a probability distribution of the quadrature

$$X = \frac{1}{\sqrt{2}}(A + A^\dagger), \quad (1)$$

where the operator A is a linear superposition of annihilation operators a_j of N signal modes,

$$A = \sum_{j=1}^N z_j a_j. \quad (2)$$

The complex coefficients z_l fulfill normalization condition

$$\sum_{j=1}^N |z_j|^2 = 1, \quad (3)$$

which ensures validity of standard commutation relation $[A, A^\dagger] = 1$ for the operator A . Two examples of experimental setups, where the statistics of quadrature X are measured, are given in Figs. 1 and 2. Multimode homodyne tomography can be employed to investigate ultrafast internal quantum correlations of optical pulses [29,30], see Fig. 1. A train of N strong LO pulses is used to select a set of N nonmonochromatic modes from the signal pulse. The modes a_j are determined by positions and shapes of the LO pulses and the correlations of the signal pulse are probed in terms of these modes. Figure 2 illustrates a scheme for homodyne tomography of single-frequency multimode field. The desired superposition A is prepared in N -port interferometer and then it enters homodyne detector. This setup can be used e.g. for measurement of a polarization state of an optical field [37]. The modes a_1 and a_2 then correspond to two orthogonal linear polarizations. The two-mode unitary transformations $U(\theta, \psi)$ leading to superpositions (2) can be performed with the help of two phase shifters and a polarizing beam splitter [37]. A common feature of the experimental setups shown in Figs. 1 and 2 is that only one balanced homodyne detector is needed.

If the statistics $w(X; \{z_j\})$ of the quadrature X are known for all $\{z_j\}$ fulfilling (3), then we have a complete

knowledge of the quantum state of the multimode light field and all quantities of interest, such as various quasidistributions, density matrix elements, and s -ordered moments, can be unambiguously determined from the distributions $w(X; \{z_j\})$.

A. Sampling of the smoothed Wigner functions

Let us begin with reconstruction of the multimode s -parametrized quasidistributions. It is convenient to work in the hyperspherical coordinates. The points $\{z_j\}$ lie on a surface of $2N$ -dimensional unit sphere and we parametrize them as [32]

$$z_j = u_j(\boldsymbol{\theta})e^{-i\psi_j}, \quad (4)$$

where

$$u_j(\boldsymbol{\theta}) = \cos\theta_j \prod_{l=1}^{j-1} \sin\theta_l, \quad j < N \quad (5)$$

$$u_N(\boldsymbol{\theta}) = \prod_{l=1}^{N-1} \sin\theta_l, \quad (6)$$

and

$$\begin{aligned} \psi_j &\in [0, 2\pi], & j &= 1, \dots, N, \\ \theta_j &\in [0, \pi/2], & j &= 1, \dots, N-1. \end{aligned}$$

To simplify the notation, we define $\boldsymbol{\theta} = (\theta_1, \dots, \theta_{N-1})$ and $\boldsymbol{\psi} = (\psi_1, \dots, \psi_N)$.

Multimode characteristic function corresponding to s -ordering of the field operators is defined as [38],

$$C_s(\{\beta_j\}) = \left\langle \prod_{j=1}^N \exp\left(\frac{1}{2}s|\beta_j|^2 + \beta_j a_j^\dagger - \beta_j^* a_j\right) \right\rangle, \quad (7)$$

where $\langle \rangle$ denotes quantum mechanical average. Let us compare the exponent on the right-hand side of Eq. (7) with the quadrature $X(\{z_j\}) \equiv X(\boldsymbol{\theta}, \boldsymbol{\psi})$. We can see that $C_s(\{\beta_j\})$ is proportional to characteristic function of the quadrature distribution,

$$C_s(\{\beta_j\}) = e^{sr^2/2} \int_{-\infty}^{\infty} dX e^{i\sqrt{2}rX} w(X; \boldsymbol{\theta}, \boldsymbol{\psi}), \quad (8)$$

where $\beta_j = iru_j(\boldsymbol{\theta}) \exp(i\psi_j)$ and $r > 0$ is radial variable,

$$r^2 = \sum_{j=1}^N |\beta_j|^2.$$

Multimode quasidistribution $W_s(\{\alpha_j\})$ is a Fourier transform of the characteristic function $C_s(\{\beta_j\})$,

$$W_s(\{\alpha_j\}) = \frac{1}{\pi^{2N}} \int C_s(\{\beta_j\}) \prod_{j=1}^N d^2\beta_j e^{\beta_j^* \alpha_j - \beta_j \alpha_j^*}. \quad (9)$$

We rewrite this integral in the hyperspherical coordinates. We shall integrate over the angles θ_j , phases ψ_j , and radius r . It is convenient to introduce $d\Omega$,

$$d\Omega = g(\boldsymbol{\theta}) \prod_{l=1}^{N-1} d\theta_l \prod_{j=1}^N d\psi_j, \quad (10)$$

where the prefactor

$$g(\boldsymbol{\theta}) = \prod_{l=1}^{N-1} \cos\theta_l (\sin\theta_l)^{2(N-l)-1} \quad (11)$$

stems from the Jacobian of coordinate transformation. We substitute the characteristic function (8) into (9) and after some algebra we arrive at

$$W_s(\{\alpha_j\}) = \frac{1}{\pi^{2N}} \int_0^\infty dr \int_\Omega d\Omega \int_{-\infty}^\infty dX r^{2N-1} \times e^{sr^2/2} e^{i\sqrt{2}r(X-\tilde{X})} w(X; \boldsymbol{\theta}, \boldsymbol{\psi}), \quad (12)$$

where we have introduced a c-number quadrature

$$\tilde{X}(\{\alpha_j\}, \boldsymbol{\theta}, \boldsymbol{\psi}) = \frac{1}{\sqrt{2}} \sum_{j=1}^N (u_j(\boldsymbol{\theta}) e^{-i\psi_j} \alpha_j + \text{c.c.}). \quad (13)$$

After changing the order of integration in (12), we find that

$$W_s(\{\alpha_j\}) = \int_\Omega d\Omega \int_{-\infty}^\infty dX w(X; \boldsymbol{\theta}, \boldsymbol{\psi}) \times S_N(X - \tilde{X}(\{\alpha_j\}, \boldsymbol{\theta}, \boldsymbol{\psi}); s), \quad (14)$$

where the sampling function S_N reads

$$S_N(\xi; s) = \frac{1}{\pi^{2N}} \int_0^\infty dr e^{sr^2/2} e^{i\sqrt{2}r\xi} r^{2N-1}, \quad s < 0. \quad (15)$$

This expression can be further simplified. The quasidistributions $W_s(\{\alpha_j\})$ as well as the quadrature distributions $w(X; \boldsymbol{\theta}, \boldsymbol{\psi})$ are real functions. The sampling function S_N has to be real and only real part of the above integral should be considered. The imaginary part of S_N is a null function whose average over any physical quadrature distribution $w(X; \boldsymbol{\theta}, \boldsymbol{\psi})$ is zero. Thus we can replace $\exp(i\sqrt{2}r\xi)$ by $\cos(\sqrt{2}r\xi)$ in Eq. (15). The integration over r can be easily carried out and yields a confluent hypergeometric function,

$$S_N(\xi; s) = \frac{2^{N-1}(N-1)!}{\pi^{2N}|s|^N} \Phi\left(N, \frac{1}{2}; -\frac{\xi^2}{|s|}\right). \quad (16)$$

The function S_N depends on α_j , X , $\boldsymbol{\theta}$, and $\boldsymbol{\psi}$ only through a specific combination $\xi = X - \tilde{X}$.

The parameter s must be negative because the integral (15) would diverge otherwise. This implies that only smoothed Wigner functions corresponding to $s < 0$ can be directly sampled from homodyne statistics. The confluent hypergeometric functions can be expressed in terms of the error function of the imaginary argument $\text{erfi}(x)$. It holds that

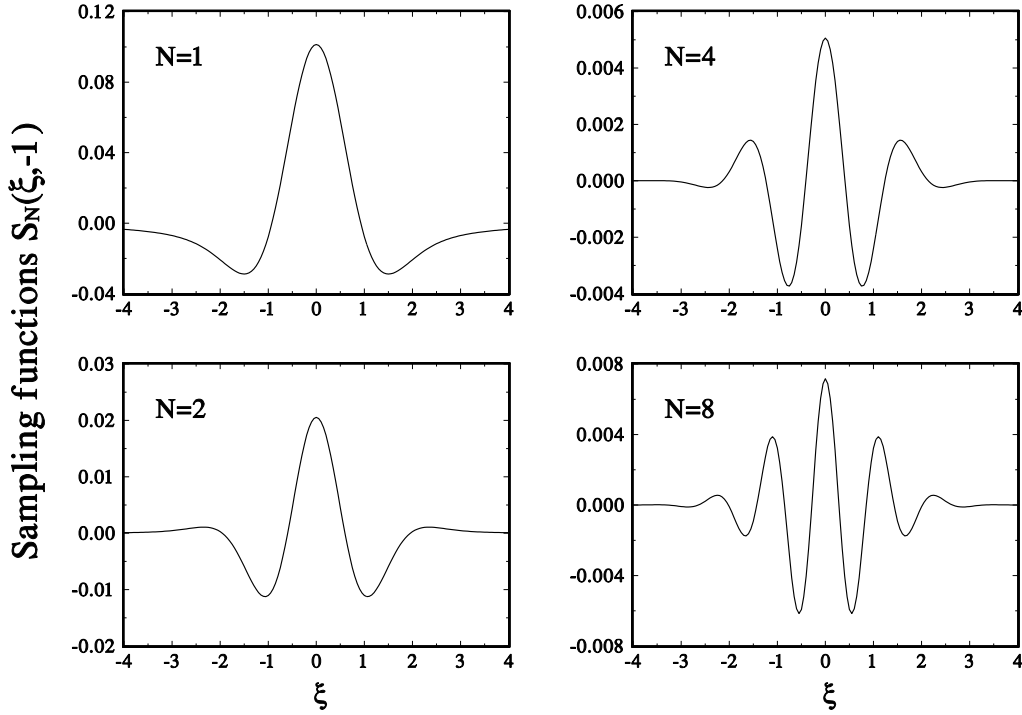


FIG. 3. Sampling functions $S_N(\xi, -1)$ for the Husimi Q -function of N -mode optical field.

$$\Phi\left(1, \frac{1}{2}; -x^2\right) = 1 - \sqrt{\pi} x e^{-x^2} \operatorname{erfi}(x),$$

$$\Phi\left(N+1, \frac{1}{2}; -x^2\right) = \frac{(-1)^N}{2^{2N} N!} \frac{d^{2N}}{dx^{2N}} \Phi\left(1, \frac{1}{2}; -x^2\right),$$

which allows for an easy determination of the required sampling function.

Our results form a multimode generalization of the single-mode relations obtained by Vogel and Risken [9] and by Richter [23]. Notice also, that D'Ariano *et al.* gave explicit formula for sampling function of two-mode Husimi quasidistribution [32]. Several functions $S_N(\xi; -1)$ are plotted in Fig. 3. The number of oscillations of $S_N(\xi; s)$ increases with increasing N and the sampling functions are bounded, $S_N \rightarrow 0$ as $|\xi| \rightarrow \infty$.

B. Imperfect detection and loss-compensating sampling functions

The sampling functions (16) would yield correct results only in the ideal case of unit detection efficiency. In a realistic experiment, losses are inevitable and the overall detection efficiency η is lower than 1. The losses can be modeled as a mixing of the signal mode with a vacuum on a beam splitter. The detected quadrature X' is thus a superposition of the original quadrature X and a vacuum-state quadrature X_{vac} [39],

$$X' = \sqrt{\eta}X + \sqrt{1-\eta}X_{\text{vac}}. \quad (17)$$

With the help of (17) one can find a simple relation between the characteristic functions of the quadratures X and X' ,

$$\left\langle \exp\left(i\sqrt{2}rX\right) \right\rangle = \exp\left(\frac{1-\eta}{2\eta}r^2\right) \left\langle \exp\left(i\sqrt{\frac{2}{\eta}}rX'\right) \right\rangle. \quad (18)$$

Inserting formula (18) into (8) and repeating the steps leading to Eq. (16) one finds that the replacements

$$s \rightarrow s + \frac{1-\eta}{\eta}, \quad X \rightarrow \frac{X}{\sqrt{\eta}} \quad (19)$$

are necessary and sufficient in Eq. (14) to account for detection losses,

$$S_N\left(X, \tilde{X}; s, \eta\right) = S_N\left(\frac{X}{\sqrt{\eta}} - \tilde{X}; s + \frac{1-\eta}{\eta}\right). \quad (20)$$

The losses impose a new limit on the ordering parameter s because the modified ordering parameter $s + (1-\eta)/\eta$ must be negative,

$$s < -\frac{1-\eta}{\eta} \equiv s_\eta. \quad (21)$$

Only smoothed Wigner functions with $s < s_\eta$ can be reconstructed if losses are present in the experiment.

III. DENSITY MATRIX ELEMENTS

In this section we briefly address the sampling of multimode density matrix elements in the Fock state basis $|\{n_l\}\rangle = |n_1\rangle|n_2\rangle \dots |n_N\rangle$,

$$\rho_{\mathbf{mn}} = \langle \{m_l\} | \rho | \{n_l\} \rangle, \quad (22)$$

where $\mathbf{m} = m_1, \dots, m_N$ and $\mathbf{n} = n_1, \dots, n_N$ are vector indices used for notation simplicity. In tomography with single LO the matrix elements $\rho_{\mathbf{mn}}$ can be reconstructed from the measured data according to

$$\rho_{\mathbf{mn}} = \int_{\Omega} d\Omega \int_{-\infty}^{\infty} dX f_{\mathbf{mn}}(X, \boldsymbol{\theta}, \boldsymbol{\psi}) w(X; \boldsymbol{\theta}, \boldsymbol{\psi}). \quad (23)$$

The functions $f_{\mathbf{mn}}$ were expressed in terms of integrals in Ref. [32]. Well-known analytical formulas for single-mode

sampling functions f_{mn} involve products of regular and irregular eigenfunctions of the harmonic oscillator Hamiltonian [14,15]. The two-mode functions $f_{m_1 m_2, n_1 n_2}$ can be written as finite series of the confluent hypergeometric functions [28]. Here we show how to derive analytical expressions for arbitrary sampling functions $f_{\mathbf{mn}}$ for generic N -mode optical field. Our starting point shall be multimode Husimi Q -function,

$$Q(\{\alpha_j\}) = \frac{1}{\pi^N} \langle \{\alpha_j\} | \rho | \{\alpha_j\} \rangle, \quad (24)$$

where $|\{\alpha_j\}\rangle$ is multimode coherent state. When the density operator ρ is expanded in Fock basis the Eq. (24) takes the form

$$Q(\{\alpha_j\}) = \frac{1}{\pi^N} \sum_{m_1, n_1=0}^{\infty} \dots \sum_{m_N, n_N=0}^{\infty} \rho_{\mathbf{mn}} \prod_{j=1}^N \frac{\alpha_j^{*m_j} \alpha_j^{n_j}}{\sqrt{m_j! n_j!}} e^{-|\alpha_j|^2}. \quad (25)$$

From this expansion we can readily see that Husimi quasidistribution $Q(\{\alpha_j\}) \equiv W_{-1}(\{\alpha_j\})$ is a generating function of the density matrix elements in Fock basis,

$$\rho_{\mathbf{mn}} = \pi^N \prod_{j=1}^N \frac{1}{\sqrt{m_j! n_j!}} \frac{\partial^{m_j}}{\partial \alpha_j^{*m_j}} \frac{\partial^{n_j}}{\partial \alpha_j^{n_j}} \left[Q(\{\alpha_j\}) \prod_{l=1}^N e^{|\alpha_l|^2} \right] \Big|_{\alpha_j = \alpha_j^* = 0}. \quad (26)$$

It follows immediately that the sampling function for the Husimi quasidistribution is a generating function of the sampling functions $f_{\mathbf{mn}}$. This can be shown explicitly by inserting the expressions (14) and (23) into Eq. (26) and comparing left- and right-hand sides of the resulting formula. We have

$$f_{\mathbf{mn}}(X, \boldsymbol{\theta}, \boldsymbol{\psi}; \eta) = \pi^N \prod_{j=1}^N \frac{1}{\sqrt{m_j! n_j!}} \frac{\partial^{m_j}}{\partial \alpha_j^{*m_j}} \frac{\partial^{n_j}}{\partial \alpha_j^{n_j}} \left[S_N \left(X, \tilde{X}(\{\alpha_j\}, \boldsymbol{\theta}, \boldsymbol{\psi}); s = -1, \eta \right) \prod_{l=1}^N e^{|\alpha_l|^2} \right] \Big|_{\alpha_j = \alpha_j^* = 0}. \quad (27)$$

This expression is general, i.e. valid for any number of modes. The Q -function can be sampled only if the detection efficiency $\eta > 0.5$, c.f. Eq. (21). This also limits the possibility of sampling the density matrix elements; the functions $f_{\mathbf{mn}}$ exist only for $\eta > 0.5$.

The dependence of $f_{\mathbf{mn}}$ on phases ψ_j can be seen from Eq. (27) even without going into explicit calculations. With the help of the substitution $\alpha_j = \gamma_j \exp(i\psi_j)$ one obtains

$$f_{\mathbf{mn}}(X, \boldsymbol{\theta}, \boldsymbol{\psi}; \eta) = F_{\mathbf{mn}}(X, \boldsymbol{\theta}; \eta) \prod_{j=1}^N e^{i(m_j - n_j)\psi_j}, \quad (28)$$

moreover, $F_{\mathbf{mn}}(X, \boldsymbol{\theta}; \eta)$ are real functions. Analytical formula for these so-called pattern functions $F_{\mathbf{mn}}$ can be derived if one inserts the sampling function S_N (16) into (27) and performs the necessary differentiations. After a tedious but straightforward calculation one finds that

$F_{\mathbf{mn}}$ can be written in terms of finite series of confluent hypergeometric functions,

$$\begin{aligned} F_{\mathbf{mn}}(X, \boldsymbol{\theta}; \eta) &= \frac{2^{N-1}}{\pi^N} \left(\frac{\eta}{2\eta - 1} \right)^N \\ &\times \prod_{j=1}^N \sqrt{\frac{\nu_j!}{\mu_j!}} \left[\sqrt{\frac{2\eta}{(2\eta - 1)}} u_j(\boldsymbol{\theta}) \right]^{\mu_j - \nu_j} \\ &\times \sum_{k_1=0}^{\nu_1} \dots \sum_{k_N=1}^{\nu_N} \Xi_N \left(\frac{X}{\sqrt{2\eta - 1}}, p_{\boldsymbol{\mu}, \boldsymbol{\nu}, \mathbf{k}} \right) \\ &\times \prod_{l=1}^N \frac{1}{k_l!} \binom{\mu_l}{\nu_l - k_l} \left[\frac{2\eta}{(2\eta - 1)} u_l^2(\boldsymbol{\theta}) \right]^{k_l}, \end{aligned} \quad (29)$$

where $\mu_j = \max(m_j, n_j)$, $\nu_j = \min(m_j, n_j)$,

$$p_{\boldsymbol{\mu}, \boldsymbol{\nu}, \mathbf{k}} = \sum_{j=1}^N \mu_j - \nu_j + 2k_j, \quad (30)$$

and

$$\Xi_N(x, 2k) = (-1)^k (N+k-1)! \Phi\left(N+k, \frac{1}{2}; -x^2\right),$$

$$\Xi_N(x, 2k+1) = 2x(-1)^k (N+k)! \Phi\left(N+k+1, \frac{3}{2}; -x^2\right).$$

Notice an interesting analogy. The quantum state is uniquely and completely determined by its Husimi quasidistribution, which contains complete information on all density matrix elements $\rho_{\mathbf{mn}}$. Similarly, all the sampling functions for density matrix elements can be obtained from the sampling function S_N , which contains all information on $f_{\mathbf{mn}}$.

A single-mode version of the formula (26) was used in [10] to find the sampling functions for single-mode density matrix elements. However, the sampling function S_N was not explicitly given in [10] and the results were written in form of complicated series. Thus later different techniques have been adopted to calculate F_{mn} [12–15]. We emphasize that for $N = 1$ the Eq. (29) yields exactly the single-mode pattern functions F_{mn} given in [12,14] and for $N = 2$ we get the two-mode pattern functions derived in [28]. The formula (29) is also suitable for investigation of the asymptotic behavior. One simply inserts the asymptotic expansions of relevant confluent hypergeometric functions into (29) and extracts the asymptotic expansion of $F_{\mathbf{mn}}$. It turns out that all pattern functions are bounded and go to zero as $|X| \rightarrow \infty$.

Finally we note that the functions $F_{\mathbf{mn}}$ given by (29) differ from those obtained in Ref. [32] because we have removed a superfluous imaginary part of S_N . Had we retained this imaginary part, we would have obtained the pattern functions derived in [32]. To see this, one can insert the integral representation (15) into Eq. (27) and differentiate prior to the integration. One recovers the formula (13) of Ref. [32],

$$F_{\mathbf{mn}}(X, \boldsymbol{\theta}; \eta) = \frac{1}{\pi^N} \prod_{j=1}^N \sqrt{\frac{\nu_j!}{\mu_j!}} [-iu_j(\boldsymbol{\theta})]^{\mu_j - \nu_j}$$

$$\times \int_0^\infty dr e^{\frac{1-2\eta}{2\eta} r^2} e^{i\sqrt{2/\eta} r X} r^{2N-1}$$

$$\times \prod_{l=1}^N r^{\mu_l - \nu_l} L_{\nu_l}^{\mu_l - \nu_l} [r^2 u_l^2(\boldsymbol{\theta})], \quad (31)$$

where $L_n^\alpha(x)$ denotes generalized Laguerre polynomial. A real part of the complex function (31) coincides with Eq. (29).

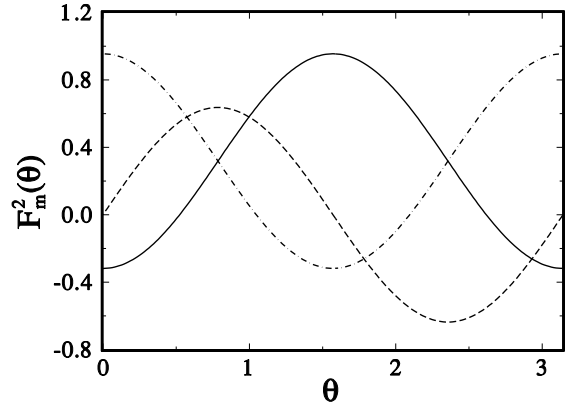


FIG. 4. The functions $F_m^2(\theta)$ biorthogonal to $G_k^2(\theta)$ in the interval $[0, \pi]$; $m = 0$ solid line, $m = 1$ dashed line, $m = 2$ dot-dashed line.

IV. S-ORDERED MOMENTS

A. Multimode sampling functions

Here we consider direct sampling of the multimode s -ordered moments

$$C_{\mathbf{mn}}^{(s)} = \langle a_1^{\dagger m_1} \dots a_N^{\dagger m_N} a_1^{n_1} \dots a_N^{n_N} \rangle_s. \quad (32)$$

We will follow an approach due to Opatrny *et al.* [29] and generalize their results for two-mode homodyning to any number of modes. The quadrature distribution $w(X; \boldsymbol{\theta}, \boldsymbol{\psi})$ can be obtained from the joint distribution $w(x_1, \dots, x_N; \boldsymbol{\psi})$ of the single mode quadratures

$$x_j = \frac{1}{\sqrt{2}} (a_j e^{-i\psi_j} + a_j^\dagger e^{i\psi_j}) \quad (33)$$

according to

$$w(X; \boldsymbol{\theta}, \boldsymbol{\psi}) = \int_{-\infty}^\infty dx_1 \dots \int_{-\infty}^\infty dx_N w(x_1, \dots, x_N; \boldsymbol{\psi})$$

$$\times \delta\left(X - \sum_{j=1}^N u_j(\boldsymbol{\theta}) x_j\right). \quad (34)$$

The moments (32) can be reconstructed from the joint quadrature statistics as follows:

$$C_{\mathbf{mn}}^{(s)} = \int w(x_1, \dots, x_N; \boldsymbol{\psi}) \prod_{j=1}^N dx_j d\psi_j \left(\frac{s}{2}\right)^{(m_j+n_j)/2}$$

$$\times H_{m_j+n_j}\left(\frac{x_j}{\sqrt{s}}\right) K(m_j, n_j) e^{i(n_j-m_j)\psi_j}, \quad (35)$$

where we integrate over N quadratures $x_j \in (-\infty, \infty)$ and N phases $\psi_j \in [0, \pi]$. $H_n(x)$ denotes customary Hermite polynomial of variable x and

$$K(m, n) = \left[\pi \binom{m+n}{n} \right]^{-1}. \quad (36)$$

The multimode sampling function employed in Eq. (35) is just a product of the appropriate single-mode sampling functions derived in [18].

We would like to link $C_{\mathbf{mn}}^{(s)}$ to the quadrature distribution $w(X; \boldsymbol{\theta}, \boldsymbol{\psi})$,

$$C_{\mathbf{mn}}^{(s)} = \int_{\tilde{\Omega}} d\tilde{\Omega} \int_{-\infty}^{\infty} dX D_{\mathbf{mn}}(X; \boldsymbol{\theta}, \boldsymbol{\psi}; s) w(X; \boldsymbol{\theta}, \boldsymbol{\psi}), \quad (37)$$

where

$$\int_{\tilde{\Omega}} d\tilde{\Omega} = \prod_{l=1}^{N-1} \int_0^{\theta_{\max}} d\theta_l \prod_{j=1}^N \int_0^{\pi} d\psi_j. \quad (38)$$

Notice the definition interval of the phase variables, $\psi_j \in [0, \pi]$. The upper bound of integration over θ_j is denoted by θ_{\max} . The most straightforward choice would be, of course, to keep $\theta_{\max} = \pi/2$ as in previous sections.

As we shall see later, the choice $\theta_{\max} = \pi$ can be more suitable.

Following [29] we shall look for the sampling function $D_{\mathbf{mn}}$ in the factorized form,

$$D_{\mathbf{mn}}(X, \boldsymbol{\theta}, \boldsymbol{\psi}; s) = \left(\frac{s}{2}\right)^{M/2} H_M \left(\frac{X}{\sqrt{s}}\right) \prod_{l=1}^{N-1} F_{m_l+n_l}^{M_l}(\theta_l) \times \prod_{j=1}^N K(m_j, n_j) e^{i(n_j-m_j)\psi_j}, \quad (39)$$

where $M = \sum_{l=1}^N (m_l + n_l)$ and $F_{m_l+n_l}^{M_l}(\theta_l)$ are some yet undetermined functions. Inserting Eqs. (39) and (34) into Eq. (37) and comparing the resulting expression with (35) we conclude that the following integral equation must be fulfilled:

$$\int_0^{\theta_{\max}} d\theta_1 \dots \int_0^{\theta_{\max}} d\theta_{N-1} H_M \left(\frac{1}{\sqrt{s}} \sum_{j=1}^N x_j u_j(\boldsymbol{\theta})\right) \prod_{l=1}^{N-1} F_{m_l+n_l}^{M_l}(\theta_l) = \prod_{j=1}^N H_{m_j+n_j} \left(\frac{x_j}{\sqrt{s}}\right). \quad (40)$$

We shall need the summation rule for Hermite polynomials,

$$H_l(x_1 \cos \theta + x_2 \sin \theta) = \sum_{k=0}^l G_k^l(\theta) H_k(x_1) H_{l-k}(x_2), \quad (41)$$

where

$$G_k^l(\theta) = \binom{l}{k} (\cos \theta)^k (\sin \theta)^{l-k}. \quad (42)$$

If we use the summation rule (41) repeatedly we find that

$$H_M \left(\frac{1}{\sqrt{s}} \sum_{j=1}^N x_j u_j(\boldsymbol{\theta})\right) = \sum'_{j_1, \dots, j_N} H_{j_N} \left(\frac{x_N}{\sqrt{s}}\right) \prod_{l=1}^{N-1} G_{j_l}^{k_l}(\theta_l) H_{j_l} \left(\frac{x_l}{\sqrt{s}}\right), \quad (43)$$

which is a multimode generalization of (41). The prime denotes sum over all j_1, \dots, j_N meeting the constraint $\sum_{l=1}^N j_l = M$, and

$$k_l = \sum_{p=l}^N j_p. \quad (44)$$

The expansion (43) is inserted into Eq. (40) where the integration over θ_l should select the right sequence of the

Hermite polynomials. Let us assume that the functions $F_m^l(\theta)$ are biorthogonal to $G_k^l(\theta)$ in the interval $[0, \theta_{\max}]$,

$$\int_0^{\theta_{\max}} d\theta G_k^l(\theta) F_m^l(\theta) = \delta_{m,k}, \quad k = 0, \dots, l. \quad (45)$$

The biorthogonality property (45) ensures that the integral equation (40) is fulfilled if the indices M_l are constructed in the same way as k_l , Eq. (44), where j_p is replaced by $m_p + n_p$,

$$M_l = \sum_{p=l}^N m_p + n_p. \quad (46)$$

Indeed, the integration over θ_1 in (40) then selects correct value of the sum $m_1 + n_1$, subsequent integration over θ_2 fixes $m_2 + n_2$ and so on. Notice also that the correct values of the differences $n_j - m_j$ are fixed by the exponentials $\exp[i(n_j - m_j)\psi_j]$ in (39). The sampling functions for multimode s -ordered moments are thus given by formula (39).

The functions $F_m^l(\theta)$ biorthogonal to $G_k^l(\theta)$ have been discussed in [29]. One can construct them e.g. as linear combinations of $G_k^l(\theta)$,

$$F_m^l(\theta) = \sum_{k=0}^l A_{mk}^l G_k^l(\theta). \quad (47)$$

From the orthogonality conditions (45) one obtains a system of linear equations for the coefficients A_{mk}^l , which

can be solved for each m and l . If we choose $\theta_{\max} = \pi$, we can find simple analytical formulas for the functions F_m^l ,

$$F_m^l(\theta) = \sum_{k=0}^l e^{i(l-2k)\theta} E_{mk}^l, \quad (48)$$

where (see Appendix for derivation),

$$E_{mk}^l = \frac{i^{l-m}}{\pi} \binom{l}{k}^{-1} \sum_{j=0}^m \binom{m}{j} \binom{l-m}{k-j} (-1)^{k-j}. \quad (49)$$

The functions $F_m^2(\theta)$ are plotted in Fig. 4.

The sampling functions compensating imperfect detection $\eta < 1$, can be obtained from (39) by making use of the simple replacement (19),

$$D_{\mathbf{mn}}(X, \boldsymbol{\theta}, \boldsymbol{\psi}; s, \eta) = D_{\mathbf{mn}}\left(\frac{X}{\sqrt{\eta}}, \boldsymbol{\theta}, \boldsymbol{\psi}; s + \frac{1-\eta}{\eta}\right). \quad (50)$$

This relation is particularly simple when normally ordered moments are considered [16]. Inserting $s = 1$ into (50) we have

$$D_{\mathbf{mn}}(X, \boldsymbol{\theta}, \boldsymbol{\psi}; 1, \eta) = \eta^{-M/2} D_{\mathbf{mn}}(X, \boldsymbol{\theta}, \boldsymbol{\psi}; 1). \quad (51)$$

Normally ordered moments do not contain any contribution from vacuum fluctuations and they all vanish for a vacuum state. The experimental losses effectively reduce the value of normally ordered moment of M -th order by a factor $\eta^{M/2}$. To compensate for imperfect detection, it suffices to use the ideal sampling function as if the detection was perfect and then divide the result by $\eta^{M/2}$.

B. Effect of aliasing and reconstruction limits

In the experiment, the statistics $w(X; \boldsymbol{\theta}, \boldsymbol{\psi})$ are measured only at a certain finite number of angles $\theta_j^{(k)}$ and phases $\psi_j^{(k)}$ and the integration over $d\tilde{\Omega}$ is replaced by a summation over finite number of discrete points $(\boldsymbol{\theta}, \boldsymbol{\psi})$. This discretization imposes limits on the order of the reconstructed moments [17].

Let us first consider the phases ψ_j . To simplify the discussion as much as possible, we restrict ourselves for a while to the single-mode case and sampling of symmetrically ordered moments ($s = 0$, Weyl ordering). Let us further assume that the exact quadrature statistics are known for each of N_ψ phases $\psi^{(k)} = k\pi/N_\psi$. The sampling then reads,

$$\begin{aligned} \langle a^{\dagger m} a^n \rangle_{\text{sym}} &= \frac{\pi}{N_\psi} 2^{(m+n)/2} K(m, n) \\ &\times \sum_{k=1}^{N_\psi} \exp\left(i(n-m)\frac{k\pi}{N_\psi}\right) \int_{-\infty}^{\infty} dx x^{m+n} w\left(x, \frac{k\pi}{N_\psi}\right). \end{aligned} \quad (52)$$

The formula (52) is a discrete Fourier transform in ψ . The Fourier series of the quadrature moments,

$$\begin{aligned} \int_{-\infty}^{\infty} dx x^{m+n} w(x, \psi) &= 2^{-(m+n)/2} \\ &\times \sum_{k=0}^{m+n} \binom{m+n}{k} \langle a^{\dagger m+n-k} a^k \rangle_{\text{sym}} e^{i(m+n-2k)\psi}, \end{aligned} \quad (53)$$

contains either odd or even frequencies depending on the parity of $m+n$. The N_ψ -point discrete Fourier transform (52) gives correct results only for sufficiently low moments, because it cannot discriminate between $\exp[ik\psi]$ and $\exp[i(k+2N_\psi)\psi]$. This phenomenon is called aliasing [40] and it imposes an upper bound on the order of the reconstructed moment. When we substitute Fourier expansion (53) into Eq. (52), we find that $m < N_\psi$ and $n < N_\psi$ must hold simultaneously. The same limitation obviously holds for any s -ordering and also for multimode moment reconstruction with sampling functions $D_{\mathbf{mn}}$. In particular,

$$m_j < N_{\psi_j}, \quad n_j < N_{\psi_j}, \quad (54)$$

must be fulfilled, where N_{ψ_j} is the number of sampling points of the phase ψ_j .

Let us proceed to the angles θ_j . For a successful reconstruction, it is crucial to meet the biorthogonality conditions (45) where the integration is replaced by summation over N_θ angles $\theta^{(n)}$,

$$\sum_{n=1}^{N_\theta} F_m^l(\theta^{(n)}) G_k^l(\theta^{(n)}) = \delta_{mk}, \quad m, k = 0, \dots, l. \quad (55)$$

If the condition (55) is violated due to discretization, then the reconstruction could be spoiled with large systematic error and the sampling would not yield reliable results. We shall prove below that the functions (48) fulfill the conditions (55) provided that the sampling points are equidistant, $\theta^{(n)} = n\pi/N_\theta$, and $l < N_\theta$ holds.

First of all we recall that the functions $G_k^l(\theta)$, Eq. (42), and $F_m^l(\theta)$, Eq. (48), can be expanded in finite Fourier series, with the highest component equal to l in both cases. Moreover, both functions contain only odd or only even Fourier components, depending on the parity of l . If $F_m^l(\theta)$ is expanded in Fourier series, then Eq. (55) becomes a summation of several discrete Fourier transforms of $G_k^l(\theta)$ (we assume $\theta^{(k)} = k\pi/N_\theta$). If $l < N_\theta$, then all discrete Fourier transforms yield the same results as the original integrations, and (55) holds exactly. The main advantage of the choice $\theta_{\max} = \pi$ is now clear. It has allowed us to find analytical expressions for the functions F_m^l which meet the discretized biorthogonality conditions (55). We remark that the functions $F_{m,n}^l \equiv F_m^l(\theta^{(n)})$ can also be constructed numerically by solving a system of Eqs. (55) for a given set of sampling points $\theta^{(n)}$ [30].

Looking at formula (39) we find the limit on the order of reconstructed multimode moments,

$$M_j < N_{\theta_j}. \quad (56)$$

We can conclude that if the quadrature statistics $w(X; \boldsymbol{\theta}, \boldsymbol{\psi})$ are measured with high accuracy, then sampling at finite number of points $(\boldsymbol{\theta}, \boldsymbol{\psi})$ provides sufficient information for the successful reconstruction of certain s -ordered moments $C_{\mathbf{mn}}^{(s)}$. If we use the sampling functions $D_{\mathbf{mn}}$ and we want to reconstruct all moments of M th order we have to measure $w(X; \boldsymbol{\theta}, \boldsymbol{\psi})$ at

$$R(M, N) = (M + 1)^{2N-1} \quad (57)$$

points $(\boldsymbol{\theta}, \boldsymbol{\psi})$ (we have the factor $M + 1$ for each of N phases ψ_j and $N - 1$ angles θ_l). This number of sampling points is sufficient, but not necessary. The M th order moments of N -mode field can be parametrized by $P(M, N)$ real numbers, where

$$P(M, N) = \binom{M + 2N - 1}{M}. \quad (58)$$

It suffices to measure the statistics $w(X; \boldsymbol{\theta}, \boldsymbol{\psi})$ at $P(M, N)$ distinct points $(\boldsymbol{\theta}, \boldsymbol{\psi})$. The appropriate sampling functions must be constructed numerically for a given set of sampling points $(\boldsymbol{\theta}, \boldsymbol{\psi})$ by inverting a system of linear equations which relates the moments $C_{\mathbf{mn}}^{(s)}$ to the moments of the quadrature statistics $w(X; \boldsymbol{\theta}, \boldsymbol{\psi})$. This approach requires less sampling points because $P(M, N) < R(M, N)$. Though many interesting questions are related to this method, e.g. how to choose the points $(\boldsymbol{\theta}, \boldsymbol{\psi})$, we do not deal with it in this paper in any more detail.

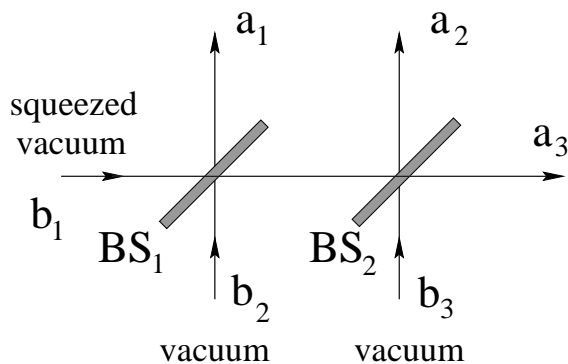


FIG. 5. Preparation of three-mode state. The squeezed vacuum in mode b_1 is mixed on beam splitters BS_1 and BS_2 with two vacua (modes b_2 and b_3), yielding the modes a_1 , a_2 , and a_3 at the outputs.

Finally, we should note that the sampling functions are not unique. This is a general feature of optical homodyne tomography. An infinite number of functions exist whose average over $w(x; \boldsymbol{\theta}, \boldsymbol{\psi})$ is zero for all physical quadrature distributions. These so-called null functions can be freely added to the above derived sampling functions. This freedom of choice is exploited in adaptive homodyne tomography to find the sampling functions minimizing statistical error for a given set of experimental data [41].

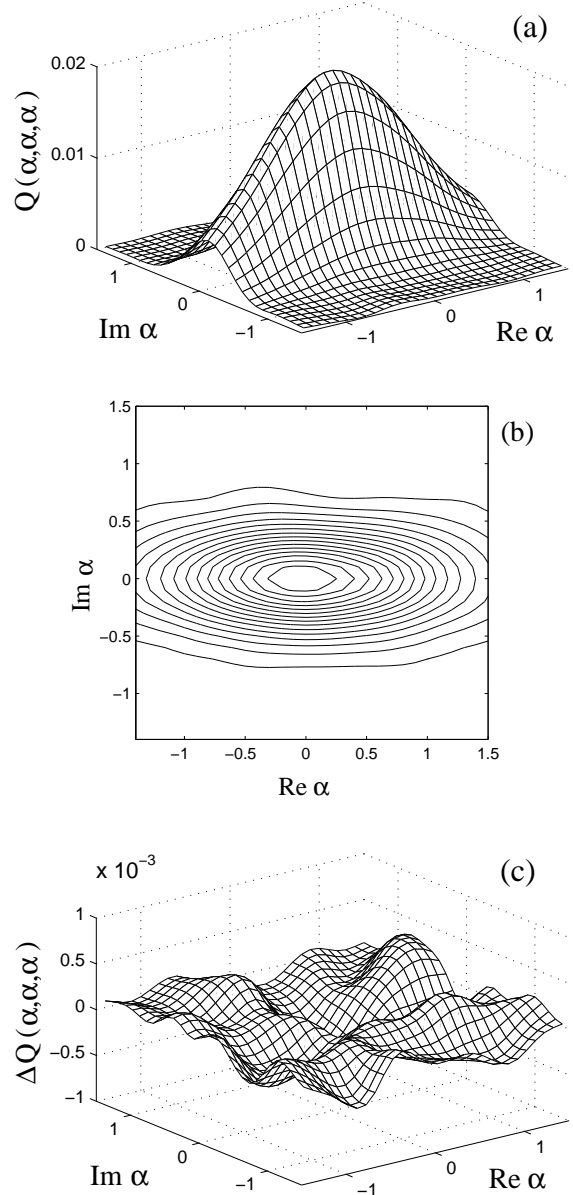


FIG. 6. Reconstruction of the three-mode Q -function of a squeezed state prepared according to Fig. 5. A two-dimensional cut $Q(\alpha, \alpha, \alpha)$ through the six-dimensional phase space is plotted. Shown are surface (a) and contour (b) plots of the reconstructed quasidistribution and a difference ΔQ between reconstructed and exact Q -functions (c).

V. MONTE CARLO SIMULATIONS

We have performed Monte Carlo simulations of multimode homodyne detection with a single LO and tested the performance of the sampling functions. Since the reconstruction of multimode density matrix elements was already considered to relatively large extent in Ref. [32], we focus here on the sampling of the multimode quasidistributions and s-ordered moments. The main purpose of this section is to illustrate the applicability of the above derived sampling functions and the feasibility of successful reconstruction of three-mode quantum state from an acceptably large amount of data.

To be more specific, we consider three-mode squeezed state prepared according to Fig. 5. This state represents a simple but nontrivial example exhibiting nonclassical properties (squeezing). As depicted in Fig. 5, single-mode squeezed vacuum in mode b_1 is mixed on two beam splitters BS_1 and BS_2 with two vacua b_2 and b_3 . The output modes

$$\begin{aligned} a_1 &= \frac{1}{\sqrt{3}}b_1 + \frac{2}{\sqrt{6}}b_2, \\ a_2 &= \frac{1}{\sqrt{3}}b_1 - \frac{1}{\sqrt{6}}b_2 - \frac{1}{\sqrt{2}}b_3, \\ a_3 &= \frac{1}{\sqrt{3}}b_1 - \frac{1}{\sqrt{6}}b_2 + \frac{1}{\sqrt{2}}b_3, \end{aligned} \quad (59)$$

can then enter the multimode homodyne detector shown in Fig. 2. The transformation (59) is unitary, thus preserving the canonical commutation relations. Moreover,

$$b_1 = b_0 \cosh r + b_0^\dagger \sinh r, \quad (60)$$

where b_0 is annihilation operator of vacuum state and r is squeezing parameter. We assume $r = 1$ in the following.

The reconstructed three-mode Q -function is shown in Fig. 6. In the computer simulation, we have sampled at 10 angles $\theta_l^{(k)} = k\pi/20$, and phases $\psi_j^{(k)} = 2\pi k/10$, $k = 1, \dots, 10$. At each point $(\boldsymbol{\theta}, \boldsymbol{\psi})$ the quadrature has been measured 50 times so that the total amount of acquired data is 5×10^6 . We have assumed a detection efficiency $\eta = 0.8$ and we have used the loss-compensating sampling function (20). $Q(\alpha_1, \alpha_2, \alpha_3)$ is a function in six-dimensional phase space, it is impossible to plot it as a whole and we must restrict ourselves to some lower-dimensional subspaces of the phase space. In Figure 6 we show a two-dimensional cut $Q(\alpha, \alpha, \alpha)$. The reconstructed Q -function exhibits Gaussian shape characteristic for squeezed states. The squeezing is clearly reflected in the elliptic shape of the Q -function, as can be seen in the contour plot in Fig. 6(b). The reconstruction error can be judged from Fig. 6(c), which depicts the difference ΔQ between exact and reconstructed Q -functions. The error is acceptably small and the reconstruction can be considered successful.

Let us now proceed to sampling the multimode moments. Again, we have assumed $\eta = 0.8$. We have

employed the loss-compensating sampling kernels (51) and the analytical functions $F_m^l(\boldsymbol{\theta})$ given by Eq. (48). We have sampled at 10 different values of each angle $\theta_l^{(k)} = k\pi/10$ and phase $\psi_j^{(k)} = k\pi/10$, $k = 1, \dots, 10$. At each point $(\boldsymbol{\theta}, \boldsymbol{\psi})$ 200 values of the quadrature X were recorded, which represents altogether 2×10^7 data.

The reconstructed normally ordered moments $\langle :n_1^k: \rangle$ and $\langle a_1^k \rangle$ can be seen in Fig. 7. The gray bars display the exact values and allow for comparison with the sampled moments. The reconstructed moments are in very good agreement with the exact values. The sampling error increases with the moment order and it is higher for $\langle a_1^k \rangle$ than for the factorial moments $\langle :n_1^k: \rangle \equiv \langle a_1^{\dagger k} a_1^k \rangle$. While $\langle :n_1^3: \rangle$ is still reconstructed with high accuracy, $\langle a_1^6 \rangle$ is sampled with certain error. This can be explained by the necessity of sampling a high Fourier component $\exp(6i\psi_1)$ in order to reconstruct $\langle a_1^6 \rangle$. When we tried to sample moments of 10th or higher orders, the results suffered from very large systematic errors because we violated the conditions (54) and (56).

The moments $\langle :n_1^k: \rangle$ contain information on the photon-number statistics of the mode a_1 . From the sampled moments we can determine the Mandel Q -parameter for j th mode,

$$Q_j = \frac{\langle :(\Delta n_j)^2: \rangle}{\langle n_j \rangle} = \frac{\langle :n_j^2: \rangle - \langle n_j \rangle^2}{\langle n_j \rangle}. \quad (61)$$

This parameter allows one to quickly distinguish between super-Poissonian ($Q_j > 0$) and sub-Poissonian ($Q_j < 0$) photon-number statistics. From the data shown in Fig. 8 we have $Q_1 \approx 1.25$ and we find that the light in the mode a_1 exhibits super-Poissonian photon number statistics. The moments of the modes a_2 and a_3 are the same as those of mode a_1 because the squeezed vacuum b_1 is equally split among the three modes a_j , c.f. Eq. (59). The sampling works equally well for the modes a_2 and a_3 and the results are very similar to those displayed in Fig. 7.

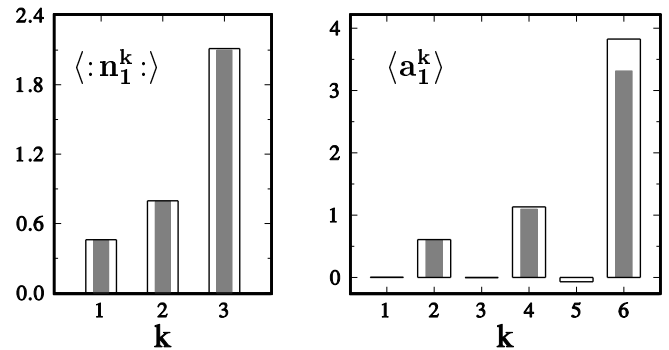


FIG. 7. Sampled moments of the mode a_1 . The empty solid bars show the reconstructed moments, the gray bars display exact values for comparison. Only real parts of the moments $\langle a_1^k \rangle$ are shown.

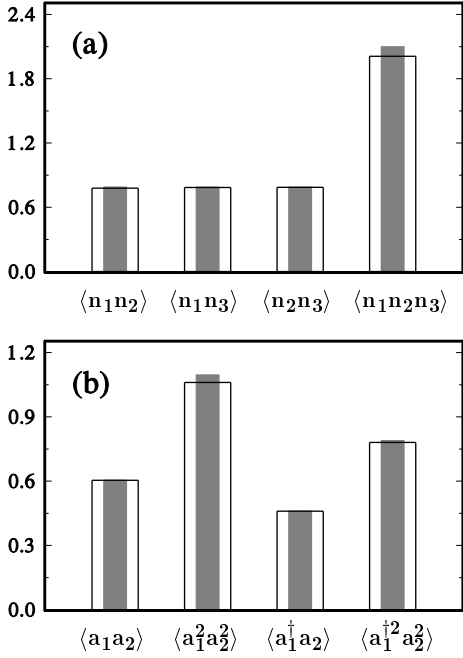


FIG. 8. Sampled two-mode and three-mode moments. In Fig. (b), real parts of the complex moments are displayed.

Having verified the feasibility of reconstruction of the single-mode moments we have finally sampled the multimode moments. Several results are shown in Fig. 8. Again, the low-order moments are reproduced with high accuracy, and the error increases with the moment order. It is worth noting that the photon number correlations

$$\langle n_1^{k_1} n_2^{k_2} \dots n_N^{k_N} \rangle_s \quad (62)$$

can be sampled from phase averaged data. This is important from the experimental point of view, because the sampling of moments (62) does not require stable relative phase between the local oscillator and signal modes. All phases ψ_j can be fully randomized, e.g., by means of randomly driven piezoelectric modulators, and the homodyning then yields phase-averaged quadrature statistics [30].

In addition to the squeezed-vacuum state discussed here, we have also considered other quantum states, such as multimode coherent states and multimode squeezed coherent states. In all cases, the reconstruction procedure worked well. The numerical simulations clearly demonstrate the feasibility of three-mode homodyne tomography from $\approx 10^7$ recorded data. Of course, the number of necessary data inevitably increases with the number of modes.

VI. CONCLUSIONS

We have derived various important sampling functions for multimode homodyne tomography with a single local oscillator. Starting from the relation between multimode characteristic function and measured quadrature

distribution we have found sampling functions for the s -parametrized quasidistributions with $s < s_\eta \leq 0$. We have proved that the sampling function for Husimi quasidistribution is a generating function of the sampling functions $f_{\mathbf{mn}}$ for density matrix elements in Fock basis $\rho_{\mathbf{mn}}$. The functions $f_{\mathbf{mn}}$ were expressed as finite series of confluent hypergeometric functions. Finally, we have found the functions allowing for direct reconstruction of multimode s -ordered moments from the homodyne data. In all cases, loss-compensating sampling functions, applicable to a realistic experiment with detection efficiency $\eta < 1$, have been provided. In order to test performance of the sampling functions we simulated homodyne detection of squeezed three-mode state and reconstructed the three-mode Q -function and several normally ordered moments. The reconstruction has shown very good results for a detection efficiency $\eta = 0.8$ and 10^7 sampled data, which is experimentally feasible. We emphasize that the multimode quantum state is reconstructed from the statistics of a class of single-mode quadratures. Only one homodyne detector is needed, which substantially simplifies the experiment. This method is particularly suitable for the measurement of ultrafast internal correlations of optical pulses or for the reconstruction of the quantum state of multimode single-frequency optical field.

ACKNOWLEDGMENTS

The author would like to thank T. Opatrný, J. Peřina, and D.-G. Welsch for stimulating and helpful discussion. Financial support of the U.S.-Israel Binational Science Foundation (Grant No. 96-00432) is gratefully acknowledged.

APPENDIX:

Here we derive the expression (48) for the functions $F_m^l(\theta)$. We insert the explicit form (42) of the function $G(\theta)$ into (45), multiply by $\alpha^k (i\beta)^{l-k}$ and sum over k ,

$$\sum_{k=0}^l \int_0^\pi \binom{l}{k} (\alpha \cos \theta)^k (i\beta \sin \theta)^{l-k} F_m^l(\theta) d\theta = \alpha^m (i\beta)^{l-m} \quad (A1)$$

The summation on the left-hand side is trivial and yields

$$\int_0^\pi (\alpha \cos \theta + i\beta \sin \theta)^l F_m^l(\theta) d\theta = \alpha^m (i\beta)^{l-m}. \quad (A2)$$

In the next step we change variables, $\delta = (\alpha + \beta)/2$, $\gamma = (\alpha - \beta)/2$ and we have

$$\int_0^\pi (\delta e^{i\theta} + \gamma e^{-i\theta})^l F_m^l(\theta) d\theta = (\gamma + \delta)^m [i(\delta - \gamma)]^{l-m}. \quad (\text{A3})$$

Now we set $\delta = 1$, differentiate (A3) k -times with respect to γ and then set $\gamma = 0$. After little algebra we arrive at

$$\int_0^\pi e^{i(l-2k)\theta} F_m^l(\theta) d\theta = i^{l-m} \frac{(l-k)!}{l!} \frac{d^k}{d\gamma^k} [(1+\gamma)^m (1-\gamma)^{l-m}] \Big|_{\gamma=0}. \quad (\text{A4})$$

Now we assume that the function F_m^l can be written in terms of finite Fourier series,

$$F_m^l(\theta) = \sum_{n=0}^l e^{i(l-2n)\theta} E_{mn}^l, \quad (\text{A5})$$

and insert this expansion into (A4). After integration on the left-hand side and differentiation on the right-hand side of (A4) we find

$$E_{mn}^l = \frac{i^{l-m}}{\pi} \binom{l}{n}^{-1} \sum_{j=0}^m \binom{m}{j} \binom{l-m}{n-j} (-1)^{n-j}, \quad (\text{A6})$$

and we have derived the formulas (48) and (49).

[1] D.T. Smithey, M. Beck, M.G. Raymer, and A. Faridani, Phys. Rev. Lett. **70**, 1244 (1993).
[2] G. Breitenbach, T. Müller, S.F. Pereira, J.-Ph. Poizat, S. Schiller, and J. Mlynek, J. Opt. Soc. Am. B **12**, 2304 (1995).
[3] S. Schiller, G. Breitenbach, S.F. Pereira, T. Müller, and J. Mlynek, Phys. Rev. Lett. **77**, 2933 (1996).
[4] M. Vasilyev, S.-K. Choi, P. Kumar, and G.M. D'Ariano, Phys. Rev. Lett. **84**, 2354 (2000).
[5] K. Banaszek and K. Wódkiewicz, Phys. Rev. Lett. **76**, 4344 (1996); S. Wallentowitz and W. Vogel, Phys. Rev. A **53**, 4528 (1996).
[6] L.G. Lutterbach and L. Davidovich, Phys. Rev. Lett. **78**, 2547 (1997); C.T. Bodendorf, G. Antesberger, M.S. Kom, and H. Walther, Phys. Rev. A **57**, 1371 (1998).
[7] T.J. Dunn, I.A. Walmsley, and S. Mukamel, Phys. Rev. Lett. **74**, 884 (1995).
[8] D. Leibfried, D.M. Meekhof, B.E. King, C. Monroe, W.M. Itano, and D.J. Wineland, Phys. Rev. Lett. **77**, 4281 (1996).
[9] K. Vogel and H. Risken, Phys. Rev. A **40** 2847 (1989).
[10] G.M. D'Ariano, C. Macchiavello, and M.G.A. Paris, Phys. Rev. A **50**, 4298 (1994).
[11] G.M. D'Ariano, U. Leonhardt, and H. Paul, Phys. Rev. A **52**, R1801, (1995).

[12] U. Leonhardt, H. Paul, and G.M. D'Ariano, Phys. Rev. A **52**, 4899 (1995).
[13] Th. Richter, Phys. Lett. A **211**, 327 (1996).
[14] U. Leonhardt, M. Munroe, T. Kiss, Th. Richter, and M.G. Raymer, Opt. Commun. **127**, 144 (1996).
[15] Th. Richter, Phys. Rev. A **61**, 063819 (2000).
[16] Th. Richter, Phys. Rev. A **53**, 1197 (1996).
[17] A. Wünsche, Phys. Rev. A **54**, 5291 (1996).
[18] Th. Richter, J. Mod. Opt. **46**, 2123 (1999).
[19] M. Dakna, T. Opatrný, and D.-G. Welsch, Opt. Commun. **148**, 355 (1998).
[20] J. Fiurášek, e-print quant-ph/0005120, Phys. Rev. A **62**, (2000), in press.
[21] D.-G. Welsch, W. Vogel, and T. Opatrný, *Homodyne detection and quantum-state reconstruction*, Progress in Optics Vol. 39, Edited by E. Wolf, (Elsevier, Amsterdam, 1999).
[22] U. Leonhardt, *Measuring the Quantum State of Light*, (Cambridge University Press, Cambridge, 1997).
[23] Th. Richter, J. Opt. B: Quantum Semiclass. Opt. **1**, 650 (1999).
[24] Z. Hradil, Phys. Rev. A **55**, R1561 (1997); Z. Hradil, J. Summhammer, and H. Rauch, Phys. Lett. A **261**, 20 (1999).
[25] V. Bužek, G. Adam, and G. Drobný, Phys. Rev. A **54**, 804 (1996).
[26] H. Kühn, D.-G. Welsch, and W. Vogel, Phys. Rev. A **51**, 4240, (1995).
[27] M.G. Raymer, D.F. McAlister, and U. Leonhardt, Phys. Rev. A **54**, 2397 (1996).
[28] Th. Richter, J. Mod. Optics **44**, 2385 (1997).
[29] T. Opatrný, D.-G. Welsch, and W. Vogel, Phys. Rev. A **55**, 1416 (1997).
[30] D.F. McAlister and M.G. Raymer, Phys. Rev. A **55**, R1609 (1997).
[31] D.F. McAlister and M.G. Raymer, J. Mod. Opt. **44**, 2359 (1997).
[32] G.M. D'Ariano, M.F. Sasaki, and P. Kumar, Phys. Rev. A **61**, 013806 (1999).
[33] J. Peřina, Z. Hradil, and B. Jurčo, *Quantum Optics and Fundamentals of Physics*, (Kluwer, Dordrecht, 1994).
[34] P.G. Kwiat, E. Waks, A.G. White, I. Appelbaum, and P.H. Eberhard, Phys. Rev. A **60**, R773 (1999).
[35] D. Bouwmeester, J.W. Pan, K. Mattle, M. Eibl, H. Weinfurter, and A. Zeilinger, Nature (London) **390**, 575 (1997); D. Boschi, S. Branca, F. De Martini, L. Hardy, and S. Popescu, Phys. Rev. Lett. **80**, 1121 (1998).
[36] T. Jennewein, Ch. Simon, G. Weihs, H. Weinfurter, and A. Zeilinger, Phys. Rev. Lett. **84**, 4729 (2000).
[37] M.G. Raymer and A.C. Funk, Phys. Rev. A **61**, 015801 (1999).
[38] J. Peřina, *Quantum statistics of linear and nonlinear optical phenomena*, (Kluwer, Dordrecht, 1991).
[39] W. Vogel and J. Grabow, Phys. Rev. A **47**, 4227 (1993).
[40] U. Leonhardt, J. Mod. Opt. **44**, 2271 (1997).
[41] G.M. D'Ariano and M.G.A. Paris, Phys. Rev. A **60**, 518 (1999).